Anton Paar

MEASURING INSTRUMENTS FOR YOUR HARD COATINGS

- Find the solution you need in our industrial portfolio, the broadest on the market
- Set up and operate our robust instruments wherever you need them, in the lab or directly at your production site
- Use reference sample kits to verify instrument performance on your own schedule, giving you results you can rely on
- Get started quicker with an application-specific support database that helps you navigate challenges

Get in touch: **www.anton-paar.com**

ADVANCED MATERIALS INTERFACES
www.advmatinterfaces.de

Real-Time Mass Change: An Intrinsic Indicator to Dynamically Probe the Electrochemical Degradation Evolution in WO_3

Zhenhua Wang, Xin Zhang, Hongliang Zhang, Fangfang Ge, Qiang Wang, Chengli Zhang, Guanglong Xu, Junhua Gao, A. A. Rogachev, and Hongtao Cao**

Although tungsten trioxide (WO_3) films are considered as the most popular inorganic electrochromic cathode, the irreversible accumulation of lithium ion in it leads to the degradation of cycling stability. In situ monitoring of mass change is critical to intrinsically probe the dynamical degradation evolution of the WO_3 films. Based on electrochemical quartz crystal microbalance analysis, a transfer model based on the migration of three mass carriers (lithium ion, perchlorate ion and propylene carbonate) is proposed. Higher potential can boost the migration of mass carriers, benefiting from the intensive driving force. Due to moderate intercalation of mass carriers and smallest difference in molar mass, the excellent electrochemical reversibility at 40 mV s^{-1} is observed. As the migration of mass carriers progresses, continuous corrosion of the WO_3 films results in electrochemical degradation. It is demonstrated that electrochemical quartz crystal microbalance-based analyses provide a valuable insight for the intercalation and extraction of mass carriers, in favor of further revealing degradation evolution induced by the irreversible intercalation of conductive ions in electrochemical devices.

1. Introduction

The migration of species at the electrochromic materials/electrolyte interface plays an imperative role in determining the electrochemical and electrochromic properties. The lithium ion (Li^+)-based electrolytes have a vast array of applications, including electrochromic devices (ECDs),[1–3] batteries,[4] capacitors,[5] and so on. It is evident that the lithium-ion trapping in the host structure would result in an electrode degradation by direct or indirect electrochemical redox in electroactive support electrolytes, giving rise to irreversible electrochemical reactions.[6–10] Generally accepted in situ or ex situ characterization techniques for probing the electrochemical degradation include electrochemical workstation,[11,12] X-ray diffraction,[13,14] optical spectroscopy,[15,16] Raman spectroscopy,[17] X-ray photoelectron spectroscopy,[18] and in situ transmission electron microscopy (TEM).[19,20] It is reported that tungsten trioxide (WO_3) shows a wide range of applications in the field of ECDs,[2] batteries,[21] capacitors,[22] photocatalysis,[23] and electrocatalytic environmental treatment,[24] owing to its reversible interfacial chemical and physical properties such as the reversible transformation from semiconductor (WO_3) to conductor (lithium tungsten bronze, Li_xWO_3) in a Li^+-based electrolyte. In terms of ECDs, the Li^+-based electrolyte can be divided into liquid,[25,26] gel,[27,28] and solid[29,30] form. So far, the lithium perchlorate ($LiClO_4$)-propylene carbonate ($C_4H_6O_3$, PC) electrolyte has been recognized as the most commonly used liquid electrolyte for WO_3-based ECDs, which still suffer from optical modulation degradation and cyclic instability. The rapid development of electrochemical workstation for monitoring the WO_3 electrodes in electrochemical process had been witnessed in the past few decades, through which the corrosion of oxide networks in the WO_3 films had been identified as a crucial contributing factor for the performance decay.[31] Recently, the electrochemical measurements coupled with optical spectroscopy have been utilized to investigate ion-trapping-induced dynamics, revealing distinct ion-trapping effects in the WO_3 films.[32] In our previous report, the degradation of the nanocrystal-in-glass WO_3 thin films has been explored by the combined technologies, partially stemming from the significant volume expansion brought by lithium-ion intercalation.[2] Due to its ability for obtaining kinetic information at interface, electrochemical impedance spectroscopy (EIS) has been reported

Z. Wang, X. Zhang, H. Zhang, F. Ge, J. Gao, H. Cao
Laboratory of Advanced Nano Materials and Devices
Ningbo Institute of Materials Technology and Engineering
Chinese Academy of Sciences
Ningbo 315201, China
E-mail: zhanghl@nimte.ac.cn; h_cao@nimte.ac.cn

H. Zhang, H. Cao
Center of Materials Science and Optoelectronics Engineering
University of Chinese Academy of Sciences
Beijing 100049, China

Q. Wang, C. Zhang, G. Xu
Ningbo Wakan Electronic Science Technology Co. Ltd
Ningbo 315475, China

A. A. Rogachev
Optical anisotropic films laboratory
Institute of Chemistry of New Materials of the National Academy of Sciences of Belarus
Minsk 220141, Belarus

The ORCID identification number(s) for the author(s) of this article can be found under https://doi.org/10.1002/admi.202200340.

DOI: 10.1002/admi.202200340

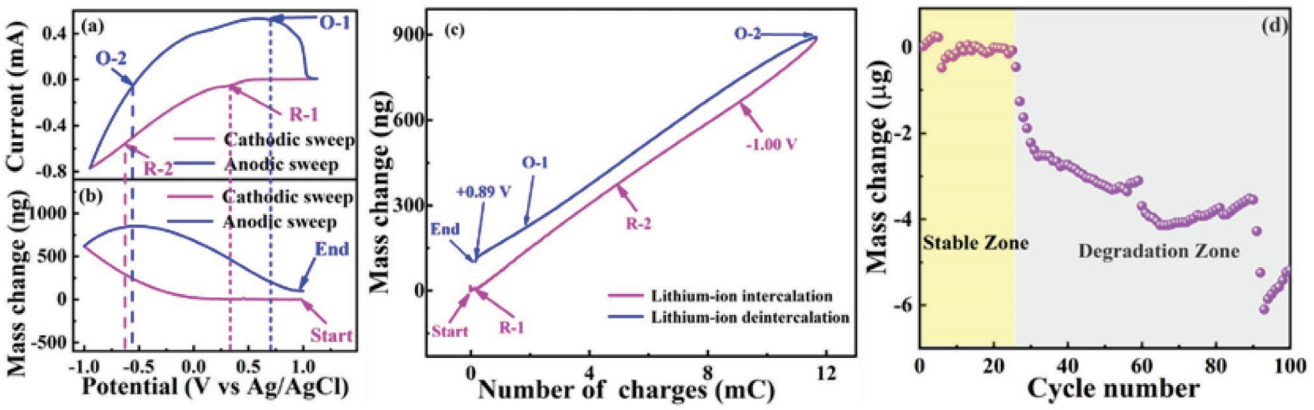

Figure 1. a) CV curve and b) related Δm plot for the WO_3 films in 0.1 M $LiClO_4$-PC electrolyte at a scan of 50 mVs^{-1}, measuring in the potential range from −1.0 to +1.0 V. c) Dependence of the number of inserted charges as a function of Δm. d) The Δm for WO_3 films at the end of each CV cycle.

for the investigation of optical degradation, demonstrating that the decrease in optical modulation can be attributed to the increasing impedance value of bleached WO_3 films at low frequencies.[33] Despite these progresses, it is still lacking in comprehensive understanding on the degradation details, such as the accurate information on the mass carriers, the transfer dynamics at the electrolyte/electrode active interface, the influence of anions (perchlorate ion, ClO_4^-), and solvent molecules ($C_4H_6O_3$) on the intercalation and extraction of lithium ion, and so on. It is generally accepted that the degradation of the WO_3 films is a dynamic process which involves mass variations during lithium-ion intercalation/extraction cycles. Therefore, to further understand the degradation mechanism of the WO_3 films, electrochemical quartz crystal microbalance (EQCM) technology as an in situ gravimetric probe can be introduced to detect the mass variations in real time.[21,34–36]

In this work, the real-time mass monitoring of the nanocrystal-in-glass WO_3 films in an open three-electrode electrochemical cell is investigated by EQCM technology. This mass observation demonstrates that mass carriers including Li^+, ClO_4^-, and $C_4H_6O_3$ are identified by the molar mass value during the charge transfer process. More importantly, the migration mechanism related to diverse mass carriers is proposed herein, in the hope of providing new perspective on electrochemical reactions at the interface of electrochemical devices.

2. Results and Discussion

2.1. Dynamic Analysis of Real-Time Mass Change

Figure 1a,b shows the cyclic voltammogram (CV) curve and Δm plot recorded for the WO_3 films with the nanocrystal-in-glass structure (see Figure S1, Supporting Information, for details) at a scan rate of 50 mV s^{-1}, measuring in 0.1 M $LiClO_4$-PC electrolyte, respectively. Two pairs of reduction (observed at +0.32 V [R-1] and −0.70 V [R-2]) and corresponding oxidation (determined at +0.69 V [O-1] and −0.58 V [O-2]) peaks can be observed during the cathodic and anodic sweep, which are excited by the redox reaction of the WO_3 films.[19,32] The mass increment is present at the potential R-1, involving a reduction reaction caused by lithium-ion intercalation. Then the mass increment rate keeps a rising trend and reaches the maximum value of 900 ng V^{-1} until to the reduction potential R-2, indicating a deep reduction reaction caused by further intercalation of lithium ions. When it sweeps to the oxidation potential O-2, the polarity of current density is changed and the mass of the WO_3 films decreases during cathodic sweep, revealing oxide reaction induced by the extraction of lithium ions. The mass increment of 98 ng is observed after the initial CV cycle, originating from the irreversible accumulation of lithium ions.[37] For clarifying the identity information of the mass carriers involved in the charge transfer process, Δm is plotted as a function of charge quantity, as shown in Figure 1c. Average M, as a key parameter for confirming the mass carriers, can be defined as the ratio between Δm and related charge quantity passing through the electrode. There are three main species in the electrolyte solution: Li^+ cation (6.94 g mol^{-1}), ClO_4^- anion (99.45 g mol^{-1}), and PC molecular ($C_4H_6O_3$, 102.09 g mol^{-1}). The theoretical M based on the intercalation and extraction of lithium ion is 6.94 g mol^{-1}. As depicted in **Table 1**, an M between 6.77 and 8.14 g mol^{-1} is obtained in the lithium-ion intercalation, while this value for lithium-ion extraction is estimated to be ≈6.07–38.49 g mol^{-1}. These results demonstrate that other mass carriers such as ClO_4^- anion and $C_4H_6O_3$ molecular, except for Li^+ cation, are also involved in the charge transfer process. The M obtained in this study is

Table 1. The fitted average molar mass and the molar ratio of $C_4H_6O_3$ and ClO_4^- at various sweep process during CV cycle.

Potential range [V]		Molar mass [g mol^{-1}]	Molar ratio ($C_4H_6O_3$/ClO_4^-)	Average molar mass [g mol^{-1}]	Average molar ratio ($C_4H_6O_3$/ClO_4^-)
Lithium-ion intercalation	R-1→ R-2	7.49	>0.97	7.19	>0.97
	R-2→ −1.00 V	6.77	<0.97		
	−1.0 V→ O-2	8.14	>0.97		
Lithium-ion extraction	O-2→ O-1	6.74	<0.97	6.74	<0.97
	O-1→ +0.89 V	6.07	<0.97		
	+0.89V→ +1.00V	38.49	≫ 0.97		

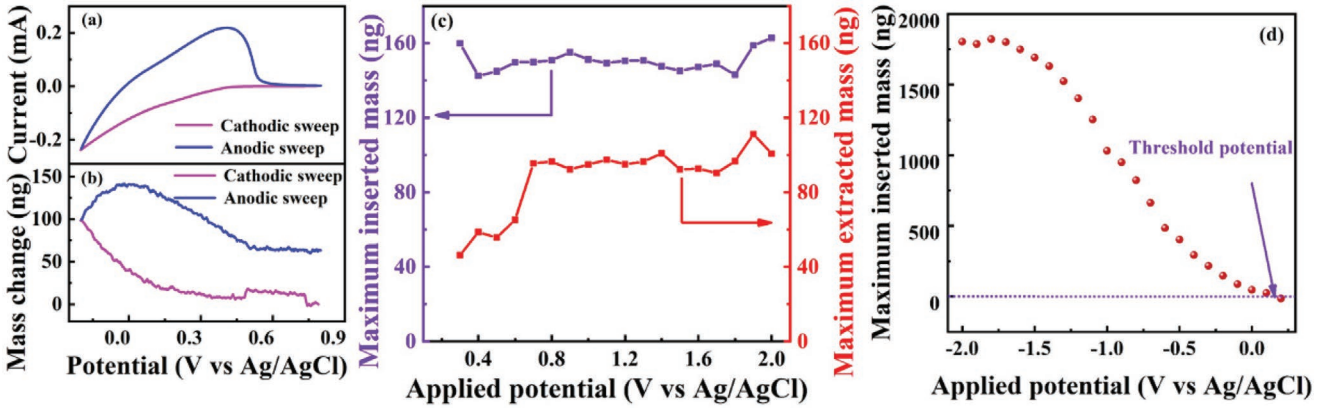

Figure 2. The influence of various potential on the lithium-ion intercalation/extraction during CV cycle. a) Cyclic voltammogram (CV) curves and b) related Δm of the WO_3 films in 0.1 M $LiClO_4$-PC electrolyte at a scan of 50 mV s^{-1}, measuring in the potential range from −0.2 V to +0.8 V. c) The maximum inserted (violet curve) and extracted (red curve) mass curve for the WO_3 films measured in various potential range (maximum positive potential varies from +0.3 to +2.0 V, holding a maximum negative potential of −0.2 V). d) The maximum inserted mass curve for the WO_3 films performed in different CV processes (maximum negative potential changes from +0.2 to −2.0 V, keeping a positive potential of +0.8 V).

mainly determined by the molar ratio between $C_4H_6O_3$ and ClO_4^-. Based on Figure 1c and Formula (2), the average M of the lithium-ion intercalation is fitted to be 7.19 g mol^{-1}, higher than that of the lithium-ion extraction (6.74 g mol^{-1}), probably owing to the facile intercalation of ClO_4^- anion uncovered by the smaller $C_4H_6O_3/ClO_4^-$ molar ratio and the irreversible intercalation of partial lithium ions. The irreversible intercalation of partial Li^+ can lead to an increase in the percentage ratio of ClO_4^- to all mass carriers during the lithium-ion extraction, causing a smaller average molar mass. The WO_3 films present a poor electrochemical cycling stability, as reflected by the noncoincident CV curves in Figure S2a, Supporting Information. To investigate the electrochemical cycling stability of the WO_3 films, the Δm profile and the frequency variation plot are displayed in Figure 1d and Figure S2b, Supporting Information, respectively. Within the initial 25 cycles (Stable zone), the Δm is marginal, which can be attributed to the amorphous buffering effect on the structural collapse of the WO_3 matrix.[2] Then, the mass is dramatically decreased after initial 25 cycles (Degradation zone), leading to poor electrochemical stability.

2.2. The Influence of Applied Potentials on Mass Transfer Process

Applied potential as an important parameter to probe the charge transfer process is worthy of serious consideration. The CV curve and Δm plot in a narrow potential range from −0.2 to 0.8 V are displayed in **Figures 2**a,b, respectively. The Δm exhibits the same trend as the above one acquired under a different potential range from −1.0 to 1.0 V, with a small mass fluctuation. To further investigate the effect of applied potential on the intercalation and extraction of mass carriers, the Δm under a series of potentials is measured. Figure 2c presents the maximum inserted/extracted mass curves measured in a series of CV processes. The maximum positive potential applied on the WO_3 films as working electrode is varied from +0.3 to +2.0 V, and the maximum negative potential has a constant value of −0.2 V. The maximum inserted mass, determined to be 150.4 ng averagely, is mainly depended on the negative polarized potential, while the maximum extracted mass is increased with the increment of positive potential as a result of the time extension and external driving force for lithium-ion extraction. Nevertheless, the intercalated mass carriers cannot be extracted completely, suggesting partial ions binding to deep ion-trapping sites. Figure 2d illustrates the maximum inserted mass plot measured in different potential ranges. The maximum negative potential is changed from +0.2 to −2.0 V, keeping a maximum positive potential of +0.8 V. It can be seen that the maximum inserted mass is gradually increased to a saturation value of ≈1800 ng from +0.2 to −2.0 V, implying the finite "active sites" for the migration and storage of mass carriers (including Li^+, ClO_4^-, and $C_4H_6O_3$) in the frame structure of WO_3 films. Intriguingly, the mass increment at +0.1 and +0.2 V is estimated to be about 24.5 and −14.7 ng, respectively, inferring that a threshold potential is probably between 0.1 and 0.2 V for the lithium-ion intercalation/extraction.

2.3. Analysis of Dependence between Electrochemical Reversibility and Scan Rate

The Δm measured at various scan rates was investigated to find out the effect of scan rate on the intercalation and extraction of mass carriers. **Figures 3**a,b show the CV curves and Δm plots of the WO_3 films, respectively. As the scan rate decreases, the Δm of the WO_3 films is significantly increased. The reason for the higher Δm obtained at lower scan rate is mainly contributed to the sufficient time for lithium-ion intercalation.[38] Figure 3c illustrates the average M and the difference in M curve (ΔM) as a function of scan rate. It can be seen that the average M is drastically decreased at higher scan rates (≥60 mV s^{-1}), indicating the enhancement in the intercalation/extraction of ClO_4^- anions and the suppression of Li^+ cations and $C_4H_6O_3$ molecular. The decreased Li^+/(all mass carriers) ratio at high scan rate can reduce the Coulomb force between Li^+ cation and ClO_4^- anion during electrochemical process, which facilitates the intercalation/extraction of ClO_4^-. The ΔM mainly originated

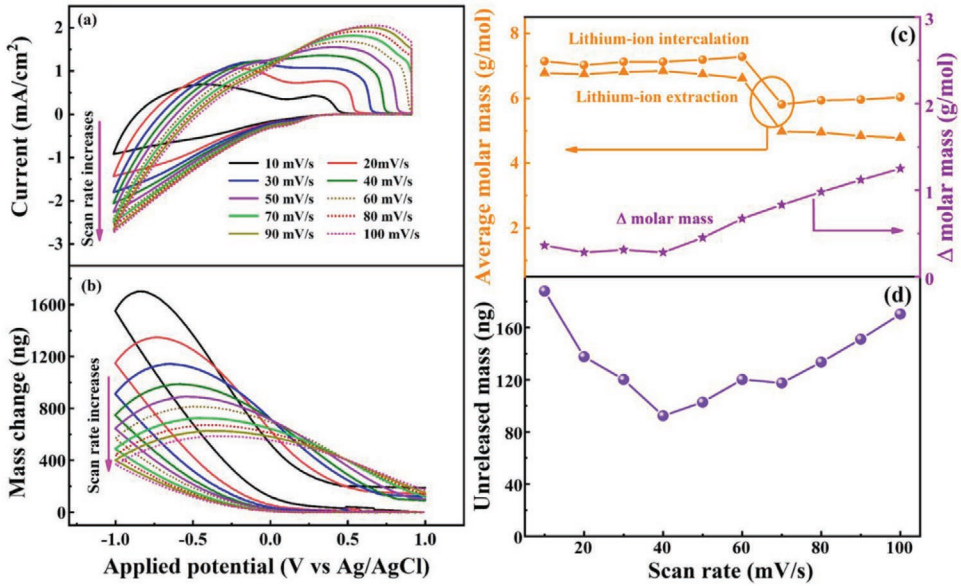

Figure 3. Investigation on the intercalation and extraction of mass carriers at various scan rates. a) CV curves and b) related Δm plots for the WO_3 films in a 0.1 M $LiClO_4$-PC electrolyte at various scan rates from 10 m to 100 mV s^{-1}. c) The average molar mass and the Δ molar mass during lithium-ion intercalation/extraction. d) Unreleased mass for the WO_3 thin films under various scan rates.

from the ClO_4^-/(all mass carriers) ratio difference between the intercalation and extraction process. The significant increment of the ΔM at higher scan rates (≥40 mV s^{-1}) suggests that ClO_4^- intercalation becomes easier than its extraction. The unreleased mass obtained at various scan rates can be used to evaluate the reversibility of the WO_3 films, as shown in Figure 3d. The irreversible trapping of Li^+ into the WO_3 films is the main origination of unreleased mass, involving an irreversible redox reaction at the electrode/electrolyte interface. The unreleased mass observed at 40 mV s^{-1} gets to the lowest value of 92.3 ng, manifesting a pretty good electrochemical reversibility, in response to minute ΔM (0.28 g mol^{-1}) and moderate scan rate. On the one hand, as the scan rate decreases (<40 mV s^{-1}), it can provide more time for the ion intercalation or even excessive intercalation, leading to relatively poor reversibility. On the other, the increment of ΔM at higher scan rates (>40 mV s^{-1}) is mainly caused by the excessive ClO_4^- intercalation, destroying the electrochemical reversibility.

2.4. Real-Time Analysis of Degradation Evolution during GCD Cycles

Capacity retention, as a key electrochemical performance, is experimentally investigated by recording the Δm during the galvanostatic charge/discharge (GCD) tests. Figure S3, Supporting Information, shows several relatively symmetrical GCD curves performed at current densities ranging from 0.50 to 1.50 mA cm^{-2}, revealing the pseudocapacitance characteristics.[39] The Δm plot and capacity retention curve for the WO_3 films operating at 1.50 mA cm^{-2} during 500 GCD cycles is illustrated in **Figures 4**a,b, respectively. In the initial 50 GCD cycles (zone I), the mass increment is companied by the decrement of capacity retention, implying that the intercalation and extraction

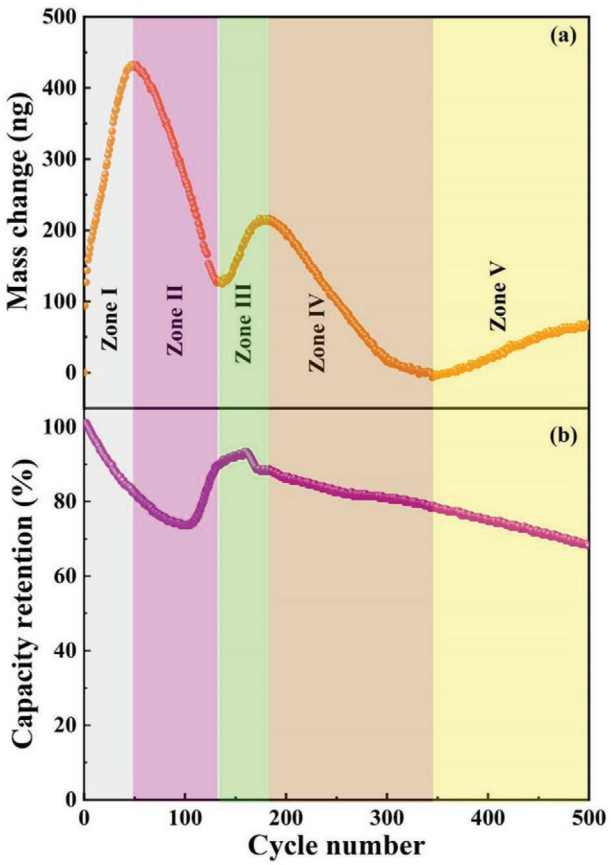

Figure 4. Evaluation of the relationship between Δm and capacity retention during galvanostatic charge/discharge (GCD) cycles. a) Δm and b) capacity retention for the WO_3 films at a current density of 1.50 mA cm^{-2} during 500 GCD cycles.

processes are hindered to some extent. Then the significant mass decrement along with a continuous decrease of capacity retention is observed during GCD cycles from 50 to 137 (zone II), owing to the structural detriment of the WO_3 film. In zone III, it is worth noting that the electrochemical activation at the Li^+-based electrolyte/WO_3 interface would cause the improvement of the capacity retention, contributing to the mass increment.[40] Afterward, the mass is gradually decreased with the detriment of the WO_3 host structure in zone IV. In zone V, however, the abnormal mass increment may be due to the absorption of film fragment peeled off from the substrate (as shown in Figure S4, Supporting Information).

2.5. Establishment of Migration Mechanism of Mass Carriers

In view of the above investigation, the following mechanism concerning the intercalation/extraction of mass carriers at the electrolyte/WO_3 interface during CV test is proposed, as described in **Figure 5**. Step I represents the slight mass decrement corresponding to the extraction of ClO_4^- anions from the matrix. These ClO_4^- anions can be easily adsorbed onto the WO_3 surface, even if positive potential is applied. Step II (reduction potential R-1) reflects that the Li^+ cations and $C_4H_6O_3$ solvent molecules are intercalating into the electrode, accompanied by the extraction of a small amount of ClO_4^- anions. At higher negative potentials (Step III, reduction potential R-2), the mass increment rate approaches a maximum value of 900 ng · V^{-1}, indicating the rapid intercalation of Li^+ cations into the WO_3 films. At the same time, the extraction of ClO_4^- anions is enhanced as well under higher negative reduction potentials. Then afterward, Li^+ cations and solvent molecules are still intercalated into the electrode during the initial stage of anodic sweep (Step IV). When it comes to oxidation potential O-2 (Step V), the mass begins to decrease. The mass decrement suggests that Li^+ cations and $C_4H_6O_3$ molecules are expelled back to the electrolyte, while ClO_4^- anions are intercalating into the electrode under the action of electric field. Step VI denotes the accelerated mass decrement, an indicator of deep lithium-ion extraction. Moreover, the smallest M of 6.07 g mol^{-1} clearly demonstrates that a larger number of ClO_4^- anions are intercalated into the WO_3 films. These results suggest that deep reduction (R-2)/oxidation (O-1) potential can not only promote Li^+ intercalation/extraction but also ClO_4^- extraction/intercalation. In VII zone, it mainly refers to the extraction of $C_4H_6O_3$ molecules, presenting a larger average M of 38.49 g mol^{-1}. These micro-dynamic analyses for mass change provide comprehensive insights into the electrochemical degradation evolution of the WO_3 thin films. Moreover, the highly sensitive EQCM introduced in this work can be broadly transferable to investigate ion migration behavior at the interface of electrochemical devices.

3. Conclusions

In summary, the real-time mass change of WO_3 films is monitored by EQCM technology to investigate the degradation mechanism based on multiple cycles of lithium-ion intercalation/extraction. There are three mass carriers (Li^+, ClO_4^-, and $C_4H_6O_3$ molecular) participated in the charge transfer process. Our findings reveal that the intercalation of Li^+ and $C_4H_6O_3$ molecules and the extraction of ClO_4^- co-contribute to the mass decrement of the WO_3 films. The reinforced negative/positive potential can provide sufficient driving force for the Li^+ intercalation/extraction, facilitating the mass increment/decrement of the WO_3 films. At a moderate scan rate (40 mV s^{-1}), the WO_3 films possess acceptable electrochemical reversibility, owing to reduced ΔM and modest transfer time for lithium-ion intercalation. As the electrochemical cycle progresses, the WO_3 films possess structure corrosion under the action of mass carrier migration, resulting in electrochemical degradation. Theoretically, our findings can provide in-depth insights into the nature of electrochemical degradation and pave the way toward electrode–electrolyte interface dynamics in H^+, Na^+, K^+, Zn^{2+}, Al^{3+}, and so on using EQCM analysis.

4. Experimental Section

Preparation of the WO_3 Thin Films: In order to ensure the consistency and reliability of this research, the WO_3 thin films were deposited on Au-coated quartz crystal by electron beam evaporation technique (MUE-ECO made in ULVAC, Japan).[2] Briefly, the WO_3 films were deposited on the Au covered AT-cut quartz crystal with 6 MHz fundamental frequency at the substrate temperatures of 200 °C. The synthesis of the WO_3 films was carried out under a background pressure of less than 2.0×10^{-3} Pa. Several pure WO_3 particles with a diameter of ≈3 mm in a tungsten crucible were bombarded by an electron beam of 10 kV in vacuum of 2.0×10^{-3} Pa. The deposition rate and thickness of thin films were 0.15 nm s^{-1} and 300 nm, respectively.

Electrochemical Quartz Crystal Microbalance Measurements: EQCM measurements coupled with electrochemical tests were conducted on a PGSTAT 204 quartz crystal microbalance (Autolab, Eco-Chemie, The Netherlands). For guaranteeing objectivity, all measurements were performed on a shock-absorbing table at a quiet night to eliminate the interference of external vibration. Some pre-measures were taken to exclude the influence from the Li^+ aggregation on the WO_3 surface caused by electrostatic adsorption, as shown in Figure S5, Supporting Information. These measurements were carried out in a three-electrode electrochemical cell. As far as the EQCM test system is concerned, Au was employed as coating layer on a quartz oscillator in these experiments (as shown in Figure S6, Supporting Information), which ensures an excellent electrical conductivity and reduces an impact of side reaction. The quartz crystal deposited with the WO_3 films, a spiral shape Au bar and an Ag/AgCl gel electrode were applied as working electrode, counter electrode, and reference electrode, respectively. 0.10 M $LiClO_4$ dissolved into PC was invoked as electrolytes. The 0.1 M Li^+-based electrolytes used in all measurements were fresh electrolytes from the same batch.

Theory and Calculations: The relationship between the frequency change of the quartz resonator (Δf) and the mass change (Δm) of electrode deposited on the crystal surface was given by Sauerbrey's equation.[41]

$$\Delta f = -\Delta C_f \times \frac{\Delta m}{S} = -\frac{2nf^2}{\sqrt{\rho_q \mu_q}} \times \frac{\Delta m}{\pi r^2} \quad (1)$$

where C_f, n, f, ρ_q, μ_q, r, and S presented the sensitivity factor of the crystal (0.0815 Hz · ng^{-1} · cm^2), the number of harmonic at which the crystal was driven (this factor was set to 1, by design), the resonant frequency of the fundamental mode of the loaded crystal (6 MHz), the density of quartz (2.648 g cm^{-3}), the shear modulus of quartz (2.94×10^{11} g cm^{-1} s^{-2}), the radius of the Au electrode deposited on quartz crystal, and the area of the active piezoelectrical crystal (cm^2),

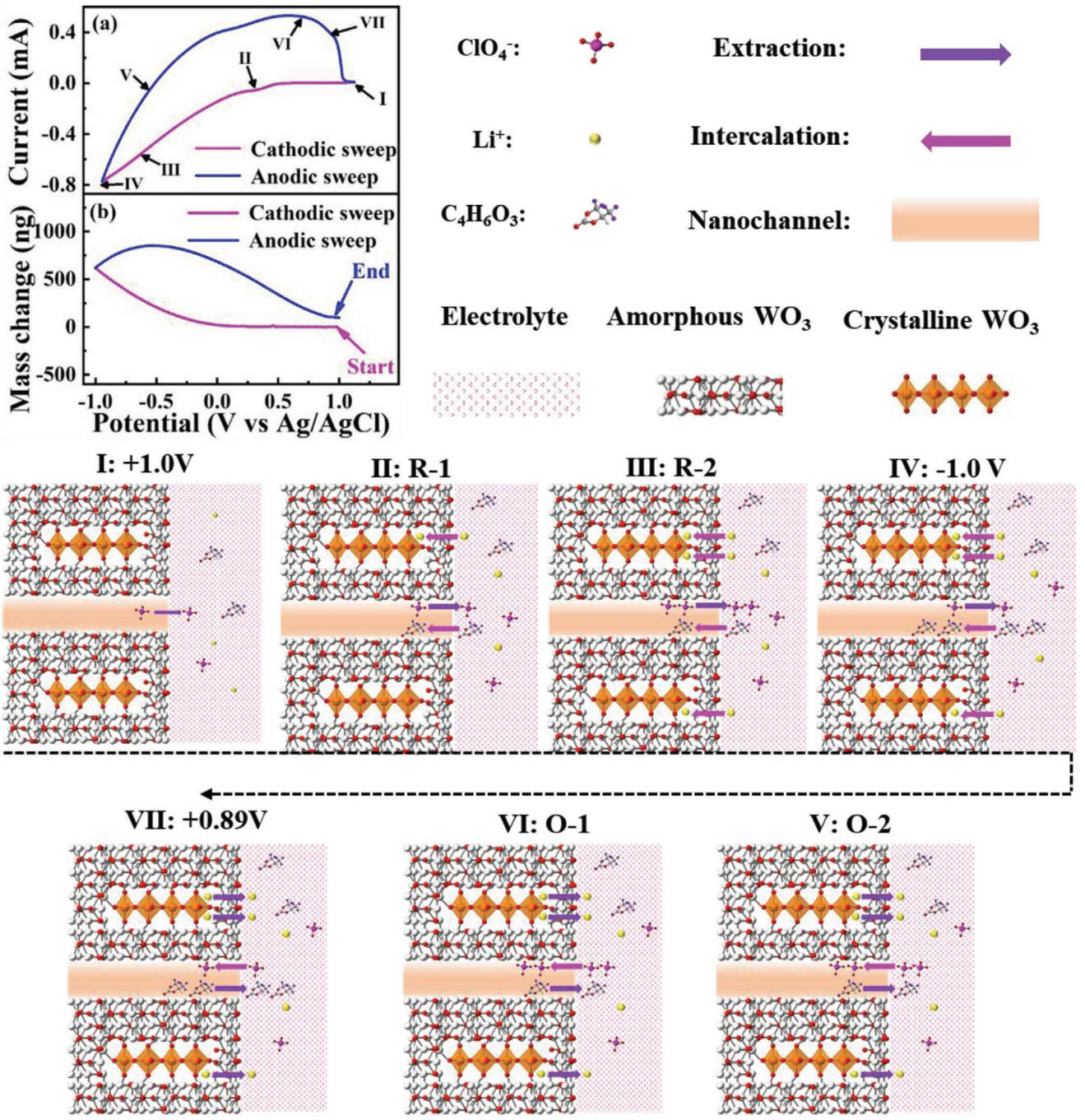

Figure 5. Scheme diagram of the intercalation and extraction of mass carriers at the 0.1 M Li^+-based electrolyte/the WO_3 films active interface occurring in three-electrode electrochemical cell.

respectively. The standard quartz crystal was 13.7 mm in diameter with a concentric disk gold-coated electrode (0.66 cm in diameter). The size (0.342 cm^2) of the device was determined by the standard Au-coated quartz crystal in our EQCM test system. An experimental value, 4.20 ng Hz^{-1}, of the calibration constant was used in this work, and the mass-to-charge ratio ($\Delta m/\Delta q$) used to estimate the molar mass (M) of the species was calculated by the following equation.[34]

$$M = \frac{nF\Delta m}{\Delta q} \quad (2)$$

where F was Faraday constant, 96 485 C mol^{-1}, n referred to the valence number of ion, and Δq (coulombs) presented the charge quantity passing through the electrode during the electrochemical process.

Supporting Information

Supporting Information is available from the Wiley Online Library or from the author.

Acknowledgements

This project was supported by the National Natural Science Foundation of China (61974148) and Ningbo Science and Technology Innovation 2025 Major Special Project (2020Z002).

Conflict of Interest

The authors declare no conflict of interest.

Data Availability Statement

Research data are not shared.

Keywords

degradation evolution, electrochemical quartz crystal microbalance, mass carriers, mass change, tungsten oxide

Received: February 13, 2022
Revised: April 28, 2022
Published online:

[1] A. Llordes, G. Garcia, J. Gazquez, D. Milliron, *Nature* **2013**, *500*, 323.
[2] D. Qiu, H. Ji, X. L. Zhang, H. L. Zhang, H. T. Cao, G. X. Chen, T. Tian, Z. Y. Chen, X. Guo, L. Y. Liang, J. H. Gao, F. Zhuge, *Inorg. Chem.* **2019**, *58*, 2089.
[3] K. Wang, H. L. Zhang, G. X. Chen, T. Tian, K. Tao, L. Y. Liang, J. H. Gao, H. T. Cao, *J. Alloy. Compd.* **2021**, *861*, 158534.
[4] C. Li, S. Wu, Y. Qiu, D. Lu, *Adv. Mater. Interfaces* **2020**, *8*, 2001588.
[5] H. Liu, L. B. Liao, Y. C. Lu, Q. Li, *Adv. Energy Mater.* **2017**, *7*, 1601248.
[6] F. Blanchard, B. Baloukas, L. Martinu, *Appl. Mater. Today* **2018**, *12*, 235.
[7] J. M. Wang, E. Khoo, P. S. Lee, J. Ma, *J. Phys. Chem. C* **2008**, *112*, 14306.
[8] X. F. Tang, G. X. Chen, H. Z. Liao, Z. X. Li, J. Zhang, J. Y. Luo, *Electrochim. Acta* **2020**, *329*, 135182.
[9] S. Hashimoto, H. Matsuoka, H. Kagechika, M. Susa, K. S. Goto, *J. Electrochem. Soc.* **1990**, *137*, 1300.
[10] R. T. Wen, G. A. Niklasson, C. G. Granqvist, *ACS Appl. Mater. Interfaces* **2015**, *7*, 28100.
[11] K. K. Purushothaman, G. Muralidharan, S. Vijayakumar, *Mater. Lett.* **2021**, *296*, 129881.
[12] Y. Yao, D. D. Sang, L. R. Zou, Q. L. Wang, C. L. Liu, *Nanomaterials* **2021**, *11*, 2136.
[13] S. L. Li, S. L. Zeng, Y. Y. Tian, X. F. Jing, F. X. Sun, G. S. Zhu, *Nano Res.* **2021**, *14*, 3288.
[14] S. Wang, H. B. Xu, T. T. Hao, P. Y. Wang, X. Zhang, H. M. Zhang, J. Y. Xue, J. P. Zhao, Y. Li, *NPG Asia Mater.* **2021**, *13*, 51.
[15] D. S. Dalavi, R. S. Devan, R. A. Patil, R. S. Patil, Y. R. Ma, S. B. Sadale, I. Kim, J. H. Kim, P. S. Patil, *J. Mater. Chem. C* **2013**, *1*, 3722.
[16] S. Sallard, T. Brezesinski, B. M. Smarsly, *J. Phys. Chem. C* **2007**, *111*, 7200.
[17] D. Chatzikyriakou, N. Krins, B. Gilbert, P. Colson, J. Dewalque, J. Denayer, R. Cloots, C. Henrist, *Electrochim. Acta* **2014**, *137*, 75.
[18] Y. Y. Liu, N. Jiang, Y. Liu, D. W. Cui, C. F. Yu, H. Q. Liu, Z. Li, *Ceram. Int.* **2021**, *47*, 22416.
[19] Z. H. Wang, G. X. Chen, H. L. Zhang, L. Y. Liang, J. H. Gao, H. T. Cao, *Scr. Mater.* **2021**, *203*, 114090.
[20] K. Qi, J. K. Wei, M. H. Sun, Q. M. Huang, X. M. Li, Z. Xu, W. L. Wang, X. D. Bai, *Angew. Chem., Int. Ed.* **2015**, *54*, 15222.
[21] H. Jiang, J. J. Hong, X. Y. Wu, T. W. Surta, Y. T. Qi, S. Y. Dong, Z. F. Li, D. P. Leonard, J. J. Holoubek, J. C. Wong, J. J. Razink, X. G. Zhang, X. L. Ji, *J. Am. Chem. Soc.* **2018**, *140*, 11556.
[22] P. A. Shinde, A. C. Lokhande, A. M. Patil, C. D. Lokhande, *J. Alloys Compd.* **2019**, *770*, 1130.
[23] Y. Jin, Z. Chen, L. Yang, K. Zhang, T. Ma, S. Zhang, W. Dai, S. Luo, *J. Alloys Compd.* **2022**, *890*, 161831.
[24] L. Yang, Z. Chen, T. Ma, S. Zhang, W. Dai, X. Xiao, X. Luo, J. Zou, X. Tu, L. Yang, S. Luo, *Chem. Eng. J.* **2021**, *412*, 127481.
[25] M. Y. Wang, H. Yu, X. Wang, X. G. Diao, *Sol. Energy Mater. Sol. Cells* **2021**, *230*, 111196.
[26] D. Choi, M. Son, T. Im, S. H. Ahn, C. S. Lee, *Mater. Chem. Phys.* **2020**, *249*, 123121.
[27] W. Y. Chen, C. Z. Zhu, L. Guo, M. Y. Yan, L. L. Wu, B. Zhu, C. J. Qi, S. Y. Liu, H. Zhang, Y. Peng, *J. Mater. Chem. C* **2019**, *7*, 3744.
[28] T. Y. Yun, X. L. Li, J. Bae, S. H. Kim, H. C. Moon, *Mater. Des.* **2019**, *162*, 45.
[29] D. M. Dong, W. W. Wang, A. Barnabe, L. Presmanes, A. Rougier, G. B. Dong, F. Zhang, H. Yu, Y. C. He, X. G. Diao, *Electrochim. Acta* **2018**, *263*, 277.
[30] L. Liu, T. Wang, Z. B. He, Y. Yi, M. Wang, Z. H. Luo, Q. R. Liu, J. L. Huang, X. L. Zhong, K. Du, X. G. Diao, *Chem. Eng. J.* **2021**, *414*, 128892.
[31] P. Judeinstein, R. Morineau, J. Livage, *Solid State Ion.* **1992**, *51*, 239.
[32] R. Wen, C. G. Granqvist, G. A. Niklasson, *Nat. Mater.* **2015**, *14*, 996.
[33] E. Pehlivan, G. A. Niklasson, C.-G. Granqvist, P. Georén, *Phys. Status Solidi A* **2010**, *207*, 1772.
[34] F. Razzaghi, C. Debiemme-Chouvy, F. Pillier, H. Perrot, O. Sel, *Phys. Chem. Chem. Phys.* **2015**, *17*, 14773.
[35] J. X. Jiang, L. Q. Qin, J. Halim, P. O. A. Persson, L. T. Hou, J. Rosen, *Nano Res.* **2021**, *15*, 3587.
[36] W. Gao, R. Demir-Cakan, H. Perrot, O. Sel, *Adv. Mater. Interfaces* **2019**, *6*, 1801855.
[37] R. T. Wen, M. A. Arvizu, M. Morales-Luna, C. G. Granqvist, G. A. Niklasson, *Chem. Mat.* **2016**, *28*, 4670.
[38] V. C. Fernandes, M. C. Santos, L. O. S. Bulhoes, *Thin Solid Films* **2007**, *515*, 7155.
[39] P. Simon, Y. Gogotsi, B. Dunn, *Science* **2014**, *343*, 1210.
[40] H. Chen, M. Zhou, Z. Wang, S. Y. Zhao, S. Y. Guan, *Electrochim. Acta* **2014**, *148*, 187.
[41] G. Sauerbrey, *Z. Phys.* **1959**, *155*, 206.